Journal of Materials Chemistry A

ROYAL SOCIETY OF CHEMISTRY

COMMUNICATION

View Article Online
View Journal | View Issue

Cite this: J. Mater. Chem. A, 2020, 8, 17951

Received 29th May 2020
Accepted 28th July 2020

DOI: 10.1039/d0ta05424k

rsc.li/materials-a

Superionic conduction in a zirconium-formate molecular solid†

Mohammad Wahiduzzaman, ‡[a] Shyamapada Nandi, ‡[a] Vibhav Yadav, [a] Kiran Taksande, [ab] Guillaume Maurin, [a] Hyungphil Chun [c] and Sabine Devautour-Vinot *[a]

The zirconium-formate molecular solid containing KCl ion pairs (ZF-3) exhibits optimum humidity-sensitive performance in terms of ionic conductivity. Molecular dynamics simulations show that the water-assisted conductivity behavior of ZF-3 results from the fast reorganization of water combined with the translational motion of Cl^-, while K^+ ions remain around their mean positions.

Solid state ionic conductors have attracted considerable attention owing to their great potential in the field of electrochemical devices for energy storage/conversion (fuel cells, electrolysers, supercapacitors and batteries) and in the environmental monitoring area (humidity/gas sensors or electrochromic windows).[1,2] Compared to their liquid analogues, they show many advantages, including a long cycle life, short charging time, environmental safety, low internal corrosion, flexibility in packaging and ability to miniaturize devices. A plethora of ion conducting materials have been identified and are classified according to their intrinsic *vs.* extrinsic disorder, amorphous *vs.* crystalline structure, bulk *vs.* interfacial control, cationic *vs.* anionic conduction and ionic *vs.* mixed ionic–electronic conduction.[3,4] Ag^+, Na^+, Li^+, O^{2-}, H^+ and F^- are the most common mobile ions present in the iconic ionic conductors,[3,4] *e.g.*, α-AgI, β-alumina, Nasicon, Lisicon, fluorite based oxides (doped zirconium dioxide), perovskite-type oxides, polymers (Nafion), *etc.* Refining known solid-state ionic conductors or developing new ones with enhanced performances is still the subject of intense activity in the field of materials science.

Molecular crystals are a versatile functional-material platform that might be of interest in the area of solid state ionics. Their structural/chemical versatility combined with appropriate flexibility of component units offers an opportunity to create a broad range of functional materials with a fine control of their 3D ordered structures at the molecular level, giving a high degree of freedom to design conduction paths for rapid ion diffusion. So far, only a very few molecular crystals have been envisaged as ionic conductors.[5–11] Typically, supramolecular solid electrolytes with Li^+ as the mobile species have been mostly considered;[5–10] however, their ionic conductivity performances are too low to rival those of traditional inorganic or polymer-based electrolyte benchmark materials.[12–14] Furthermore, the associated charge transport mechanism remains to be elucidated and this lack of fundamental understanding clearly hampers further development of this family of materials as ionic conductors. This calls for a more systematic exploration of this class of materials to assess the real potential of these solids and a deeper fundamental understanding of the microscopic mechanism which is expected to promote molecular crystals at a higher level in terms of ionic conductivity. Moreover, water was demonstrated to play a pivotal role in guest-assisting ionic conduction for diverse families of solids including zeolites, clays and MOFs *via* the formation of an extended hydrogen bond network that makes the ion transport more efficient[15–19] However, this latter strategy has never been applied so far to boost the ionic conductivity performances of molecular crystals.

Herein, we explore the ionic conductivity of ZF-3, a zirconium-formate molecular solid containing KCl ion pairs in a stoichiometric amount.[20] Remarkably, ZF-3 switches from an insulator ($\sigma = 5.1 \times 10^{-10}$ S cm^{-1} at 363 K/0% RH (Relative Humidity)) to a superionic conductor upon hydration ($\sigma = 5.2 \times 10^{-2}$ S cm^{-1} at 363 K/95% RH). This material maintains the integrity of its crystal structure under operating conditions and preserves this high level of performance over time. Molecular simulations revealed that the presence of water considerably boosts the dynamics of Cl^- species and, consecutively, the

[a]ICGM, Univ. Montpellier, CNRS, ENSCM, Montpellier, France. E-mail: sabine.devautour-vinot@umontpellier.fr

[b]Government of Maharashtra's, Ismail Yusuf College, Jogeshwari(E), Mumbai, Maharashtra, 411060, India

[c]Department of Chemical and Molecular Engineering, Hanyang University, Ansan 15588, Republic of Korea

† Electronic supplementary information (ESI) available: Experimental procedures, synthesis, PXRD, impedance data and computational details. See DOI: 10.1039/d0ta05424k

‡ These authors contributed equally to this work.

creation of Cl^-/H_2O core–shell structures throughout the pores of ZF-3. This favorable scenario is at the origin of the excellent water-assisted ionic conductivity of ZF-3.

ZF-3, with the following chemical formula $[Zr_{36}O_{24}(OH)_{48}(HCO_2)_{48}]\cdot 3KCl$, was solvothermally synthesized following the procedure previously reported (see the ESI† for details).[20] ZF-3 is composed of 6 cyclic molecular hexamers of $[Zr_6O_4(OH)_4]$ units interconnected by bridging formate ligands, resulting in a molecular structure with a hexagonal shape (Fig. 1). The zirconium-formate macrocyclic molecule consists of two types of μ-OH hydroxyl groups: (i) μ_3-OH groups belonging to the Zr_6 cluster, similar to UiO-66 type MOFs and (ii) bridging μ_2-OH groups (Zr–O(H)–Zr), as detailed in Fig. 1. These hexagonal disc-like macromolecules self-assemble into a superstructure with hollow supercages. The cohesion of the system is ensured by ion–dipole interactions involving three K^+ and Cl^- ion pairs located between adjacent hexameric $[Zr_{36}]$ clusters and by van der Waals interactions between formate ligands.

The ionic conductivity of ZF-3 was measured by complex impedance spectroscopy under anhydrous conditions at temperatures ranging from 283 K to 373 K (Fig. 2a and S2†). In the Bode representation of the conductivity *vs.* frequency, the electrical signal is mainly dominated by the polarization conductivity $\sigma'(\omega)$, while the dc conductivity plateau is only observed for the highest temperature domain ($T > 333$ K). This observation combined with a measured low conductivity value ($<10^{-9}$ S cm^{-1}) is a signature of the insulating behavior of pristine ZF-3. This means that the dynamics of the ionic species is restricted to local relaxations, while the condition for the ion diffusion over a long range is adverse. The ion hopping required for charge transport does not happen since the potential conductive ions occupy crystallographic sites that are quite far from each other. To support these experimental findings, force field Molecular Dynamics (MD) simulations were performed in the NVT ensemble at 400 K starting with the DFT-optimized empty ZF-3 structure to determine whether any free motions of K^+ and Cl^- are possible (see the ESI† for computational details). A 10 ns MD run clearly ruled out this possibility, with both ions showing only tiny displacements around their original positions as demonstrated by their corresponding Mean Square Displacement (MSD) profiles averaged over the whole MD trajectory (see ESI Fig. S8†). This restricted dynamics of both K^+ and Cl^- ions, resulting in very local motions, is consistent with the existence of strong ion–dipole interactions between these ions and the oxygen/hydrogen atoms of the μ-OH functions and the formate groups, responsible for the self-assembly of the hexameric clusters of ZF-3 (see Fig. 1).[20]

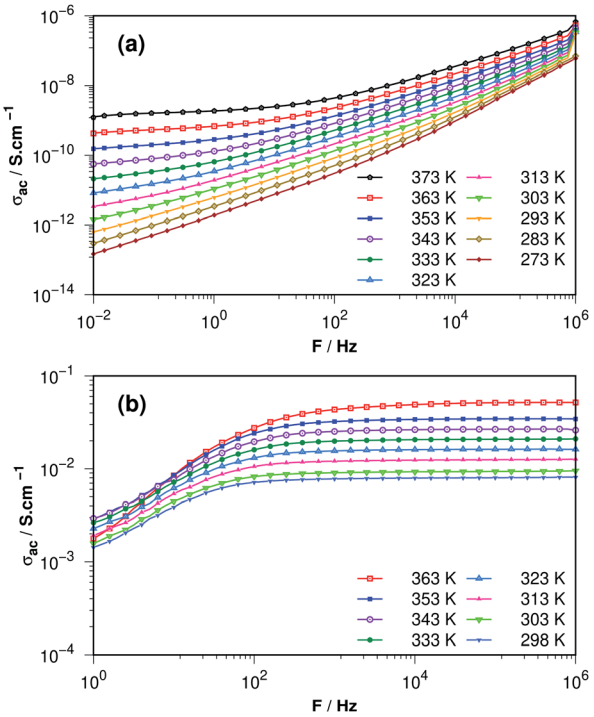

Fig. 2 Bode diagram of the conductivity for the ZF-3 powder recorded at various temperatures and at 0% (a) and 95% (b) RH.

Impedance measurements were further recorded under humid conditions (95% RH), at temperatures varying from 363 K to 298 K. Fig. 2b shows that the scenario drastically contrasts compared to the behavior recorded in the anhydrous state. At 95% RH, the conductivity profile of ZF-3 is dominated by the dc conductivity plateau (σ_{dc}), preceded by the conductivity drop in the low frequency domain which is assigned to the Maxwell Wagner Sillars response (σ_{MWS}). The σ_{MWS} contribution, due to the charge accumulation at the sample/electrode interface, reflects the ionic features of the charge carriers, while K^+, Cl^- and/or H^+ are likely to be involved in the ionic transport process. The conductivity values recorded at the dc plateau, consistent with those deduced from the Nyquist plot analysis (*cf.* Fig. S3 and Table SI†), increase from 8.0×10^{-3} S cm^{-1} to 5.2×10^{-2} S cm^{-1} when heating from 298 K to 363 K at 95% RH. These very high σ values ($\sigma > 10^{-4}$ S cm^{-1}) relate to the superconducting behavior of hydrated ZF-3.[21] This excellent level of performances, similar to that observed for the best proton conductive MOFs,[22–25] is unprecedented for a molecular crystal and makes ZF-3 as a very attractive ionic conductor under these T/RH conditions. Noteworthily, this very high conductivity is maintained over several days, *i.e.* at least 4 days (*cf.* Fig. 3a), while the structural integrity of the solid is preserved under

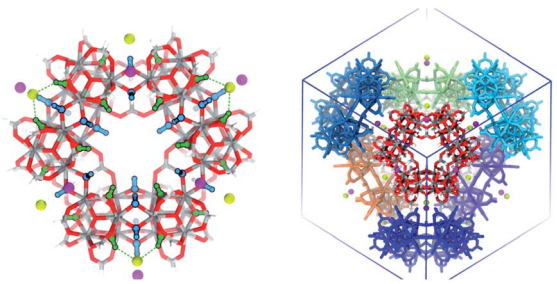

Fig. 1 Illustration of a single zirconium-formate macrocycle (left) in which the positions of hydrophilic μ_2-OH and μ_3-OH sites as well as K^+ and Cl^- ions are highlighted in blue, green, magenta and yellow spheres, respectively. The unit cell representation of ZF-3 (right), with macrocycles presented in random mono colors (except one) for an easy distinction of intermolecular arrangements.

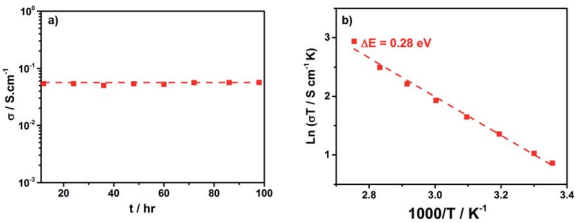

Fig. 3 Time dependence of the conductivity recorded at 363 K and 95% RH for the ZF-3 powder (a). The dashed line is a guide for the eye and corresponds to a σ value at infinite time, *i.e.* $\sigma = 0.056$ S cm^{-1}. An Arrhenius type plot of the conductivity of ZF-3 powder at 95% RH (b). The dashed line corresponds to the linear least-square fit.

operating conditions (363 K/95% RH), as confirmed by the good agreement between PXRD patterns collected for the sample before and after conductivity measurements (Fig. S1†). This emphasizes the robustness of ZF-3 upon adsorption of water vapor, which interestingly contrasts with its high solubility in liquid water.[20] This supports the fact that the macrocycles are not separated upon adsorption of water vapor, which is in line with the reversible water adsorption behavior of this molecular solid as evidenced by cyclic measurements in ref. 20. The Arrhenius plot of the conductivity measured at 95% RH ($\ln(\sigma \times T) = f(1/T)$) is illustrated in Fig. 3b and results in an activation energy ΔE of 0.28 eV. This relatively low energy value suggests an efficient transfer of the ions within the pores of the material. Impedance measurements were further carried out at 363 K under increasing RH (*cf.* Fig. S4†). A RH-conductivity dependence is clearly evidenced, with values increasing from 6.5×10^{-7} S cm^{-1} to 5.2×10^{-2} S cm^{-1} when RH rises from 35% to 95% (*cf.* Table SI†). The significant increment of the conductivity with increasing humidity unambiguously reveals that the water molecules assist the ion transport in ZF-3.

As a further stage, *ab initio* molecular dynamics (AIMD) and force field Monte Carlo (MC)/Molecular Dynamics (MD) simulations were performed to shed light on the microscopic origin of the water-assisted ionic conductivity of ZF-3. MC simulations were first performed to unravel the preferential distribution of water molecules in the pores of ZF-3 (see the ESI† for computational details). As a first stage, the reliability of the force-field we used to describe the water/host interactions was confirmed by the excellent agreement between grand canonical MC adsorption enthalpy (−62.0 kJ mol^{-1}) and the experimental isosteric heat of adsorption (−64.9 to −63.7 kJ mol^{-1}).[20] The DFT-optimized ZF-3 structure was thus loaded with ~20 wt% of water corresponding to the saturation capacity determined previously by adsorption measurements.[20] Analysis of the minimum energy MC snapshots demonstrated that water molecules preferentially form a percolated hydrogen-bonded

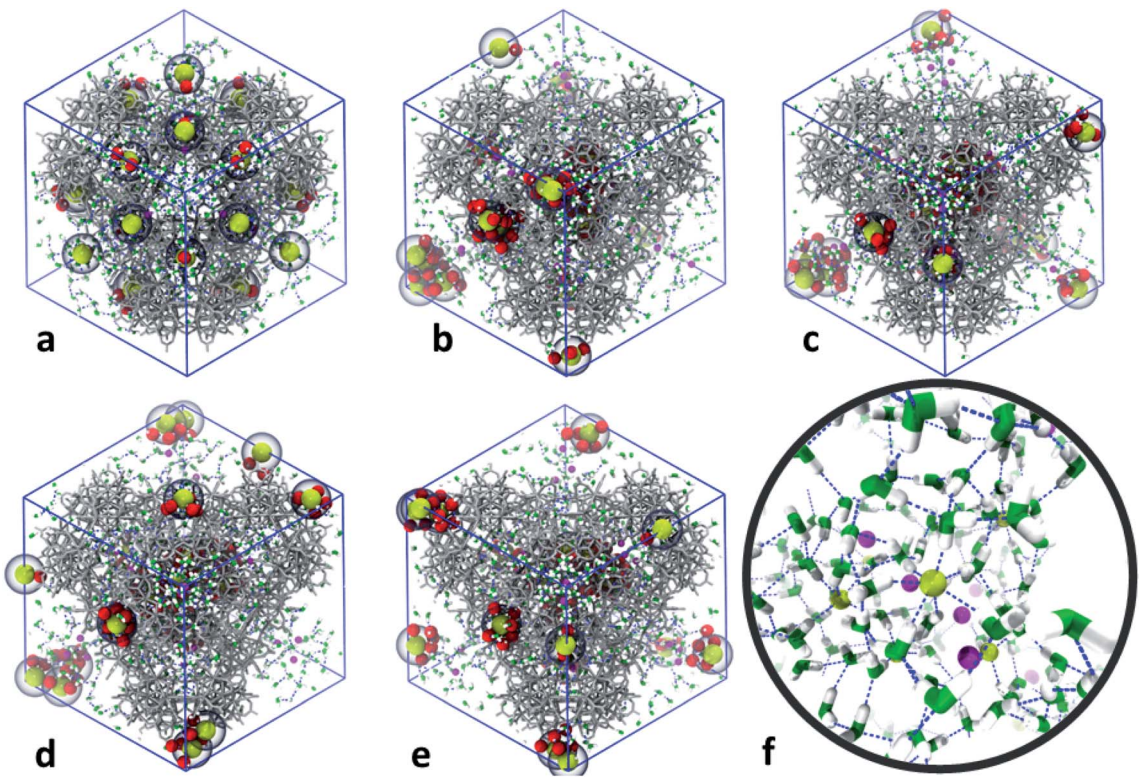

Fig. 4 Illustration of representative motions of K^+, Cl^- and H_2O captured at 0–4 ns in a 1 ns interval (a–e) from the NVT-MD simulation performed at 400 K for hydrated ZF-3. A typical molecular arrangement of a O_w–H···Cl···H–O_w water-bridge configuration where a single Cl^- ion participates in up to 7 hydrogen bonds with neighboring water molecules, is presented in (f). K^+, Cl^- and O_w atoms are represented in purple, yellow, and green spheres, respectively. The O_w atoms lying within a 4 angstrom vicinity of Cl-ions are highlighted in red and encapsulated within a transparent sphere.

network throughout the entire porosity of ZF-3 (Fig. S5†) with a corresponding mean O_w–O_w distance of 2.78 Å as seen in the radial distribution functions (RDFs) plotted for the corresponding atom pairs (Fig. S6†). This hydrogen-bonded network connects the hydrophilic μ_3-OH and μ_2-OH groups of the macrocycles as well as the free Cl^- ions (Fig. S7†). The RDFs calculated for diverse water/atom pairs evidenced that the water molecules interact more preferentially with Cl^- (higher intensity of the first RDF peak for the corresponding O_w–Cl pair) than with K^+ and both μ_3-OH and μ_2-OH functions (Fig. S6†). AIMD simulations (see the ESI† for computational details) were further conducted for the hydrated system to envisage the possible proton migration from the μ-OH functions to either H_2O or Cl^-. Typically, proton release from an acidic function grafted to a material is a relatively fast process which usually happens in a few picosecond timescale. A careful inspection of the AIMD trajectory corresponding to a 10 ps-run clearly ruled out any proton transfer. This was confirmed by the analysis of the RDF plotted for different atom pairs revealing that the O–H bond length for both μ_3-OH and μ_2-OH moieties fluctuates by only ±0.15% around its mean value ~1.0 Å while the μ-OH···O_w distance is never found to be shorter than 1.3 Å. These calculations deliver a proof that the conductivity of ZF-3 is not of a protonic nature but rather originates from the mobility of the free K^+ and Cl^- present in the pores.

Force field MD simulations were then carried out for the hydrated ZF-3 system at 400 K to probe the dynamics of both water and K^+ and Cl^- at a longer time scale. These calculations were performed starting with a minimum energy MC configuration and using the same microscopic models and parameters used in the MC simulations (see the ESI† for computational details). It appears that upon hydration, Cl^- ions undergo translational motions while K^+ ions show only local displacements around their mean positions. This is illustrated in Fig. 4 which reports the positions occupied by these ion species over a typical 4 ns range. This is further unambiguously demonstrated by the MSDs plotted for each ionic species over the MD trajectory (Fig. S9†), which show more significant motions of Cl^- *vs.* K^+, ~200 $Å^2$ and 10 $Å^2$ respectively for the 4 ns MD run. However, a moderate magnitude of the MSD for Cl^- combined with its non-linear profile over time prevents the assessment of its self-diffusion coefficient. Indeed, such dynamics refer to a medium-range mobility rather than a diffusion process as defined in the Fickian formalism. On the other hand, a quite fast long-range reorganization of the confined water molecules was evidenced. The corresponding MSD plot shows a linear regime over time (Fig. S9†). The derived self-diffusivity, D_s of 5.6 × 10^{-9} m^2 s^{-1} at 400 K using the Einstein relation[26] is significantly higher than the values usually encountered for water confined in porous materials.[27–29] A careful analysis of the MD trajectory further revealed that water preferentially forms a core–shell type configuration assembling up to 7 water molecules hydrogen bonded to a single Cl^- ion (Fig. 4). Noteworthily, the chlorine hydration shell is substantially similar to that reported in solution.[30] This H_2O/Cl^- core–shell reorganizes on very short time scales, ~50% of the water molecules in the coordination sphere of Cl^- being exchanged within a 2 ps range

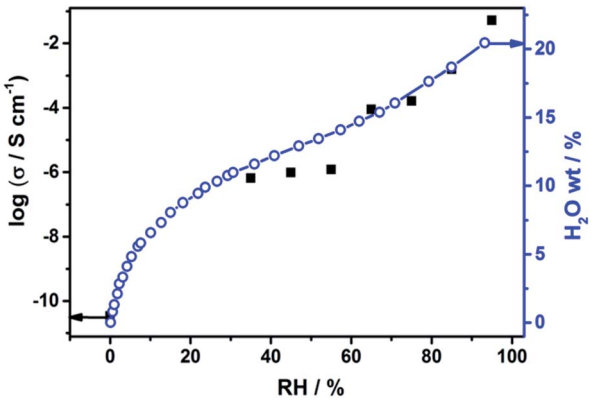

Fig. 5 Correlation between the relative humidity dependence of the conductivity recorded at 363 K and the water vapor uptake collected at 298 K for the ZF-3 powder (taken from ref. 20).

(see Fig. S10†). The dynamics of the O_w···O_w and O_w···Cl^- pairs were further assessed in terms of their hydrogen bond intermittent life times (τ_i) calculated from the corresponding time correlation functions.[31] As depicted in Fig. S11,† τ_i (O_w···O_w) was found to be about twice longer than τ_i (O_w···Cl^-) (26 ps *vs.* 10 ps). Interestingly, τ_i (O_w···O_w) is higher than the value we previously reported for water confined in a microporous MOF (47.9 ps for Y-shp-MOF-5 (ref. 32)). Such a relatively fast reorganization of water contributes to the high ion mobility within the ZF-3 porosity.

Conclusions

Because of good ionic conductivity under humid conditions, ZF-3 might be a promising candidate to be integrated in impedance-based humidity sensors. From an electrical point of view, ZF-3 is very sensitive to water, as shown by the 8 orders of magnitude gap between conductivity values recorded in the anhydrous and the hydrated states (see Table SI,† σ (363 K/0% RH) = 5.1 × 10^{-10} S cm^{-1} *vs.* σ (363 K/95% RH) = 5.2 × 10^{-2} S cm^{-1}). This sharp conductivity change with RH converges or even surpasses that recorded for other zeolite or MOF based devices already reported in the literature.[33–37] Furthermore, the conductivity dependence with RH perfectly follows the water uptake profile obtained from the volumetric adsorption isotherm (see Fig. 5).[20] The excellent correlation between conductivity and volumetric measurements highlights the good linearity response of ZF-3, one of the characteristics, along with sensitivity, to be fulfilled for considering ZF-3 with great promise for humidity sensor applications.

Author contributions

The manuscript was written through contributions of all authors. H. C. synthesized the compound. S. N., V. Y., K. T. and S.D.-V. characterized the material and performed the electrical measurements. M. W. and G. M. were in charge of the modelling.

Conflicts of interest

There are no conflicts to declare.

Acknowledgements

H. C. thanks the National Research Foundation of Korea for grant (2019R1A2C1002973 and 2016R1A5A1009405). The electrical measurements were performed with the support of the Balard Plateforme d'Analyses et de Caractérisation (PAC Balard). The authors thank Amine Geneste for technical assistance.

References

1 H. Tuller, Ionic Conduction and Applications, in *Springer Handbook of Electronic and Photonic Materials*, ed. S. Kasap and P. Capper, Boston, 2006.
2 P. R. Slater, *Encyclopedia of Materials: Science and Technology*, 2001, pp. 2848–2854.
3 K. Funke, *Sci. Technol. Adv. Mater.*, 2013, **14**, 043502.
4 O. Yamamoto, *Sci. Technol. Adv. Mater.*, 2017, **18**, 504–527.
5 T. Nakamura, T. Akutagawa, K. Honda, A. E. Underhill, A. T. Coomber and R. H. Friend, *Nature*, 1998, **394**, 159–162.
6 M. Moriya, D. Kato, W. Sakamoto and T. Yogo, *Chem.–Eur. J.*, 2013, **19**, 13554–13560.
7 M. Moriya, K. Nomura, W. Sakamotoa and T. Yogoa, *CrystEngComm*, 2014, **16**, 10512–10518.
8 M. Moriya, *Sci. Technol. Adv. Mater.*, 2017, **18**, 634–643.
9 H. Zhu, D. R. MacFarlane, J. M. Pringle and M. Forsyth, *Trends Chem.*, 2019, **1**, 126–140.
10 Y. Oki and M. Moriya, *Crystals*, 2019, **9**, 567–574.
11 C. D. Assouma, A. Crochet, Y. Choromond, B. Giese and K. M. Fromm, *Angew. Chem., Int. Ed.*, 2013, **52**, 4682–4685.
12 A. D. Sendek, G. Cheon, M. Pasta and E. J. Reed, *J. Phys. Chem. C*, 2020, **124**, 8067–8079.
13 M. Montanino, S. Passerini and G. B. Appetecchi, *Electrolytes for Rechargeable Lithium Batteries, Rechargeable Lithium Batteries from Fundamentals to Applications*, Woodhead Publishing Series in Energy, 2015, pp. 73–116.
14 Q. Li, J. Chen, L. Fan, X. Kong and Y. Lu, *Green Energy Environ.*, 2016, 1–25.
15 M. Pitman and A. C. T. van Duin, *J. Am. Chem. Soc.*, 2012, **134**, 3042–3053.
16 E. Fois and G. Tabacchi, *ChemRxiv*, 2019, DOI: 10.26434/chemrxiv.7761791.v1.
17 N. W. Ockwig, R. T. Cygan, a L. J. Criscentia and T. M. Nenoff, *Phys. Chem. Chem. Phys.*, 2008, **10**, 800–807.
18 X. Wang, Y. Wang, M. A. Silver, D. Gui, Z. Bai, Y. Wang, W. Liu, L. Chen, J. Diwu, Z. Chai and S. Wang, *Chem. Commun.*, 2018, **54**, 4429–4432.
19 S. Wang, M. Wahiduzzaman, L. Davis, A. Tissot, W. Shepard, J. Marrot, C. Martineau-Corcos, D. Hamdane, G. Maurin, S. Devautour-Vinot and C. Serre, *Nat. Commun.*, 2018, **9**, 4937.
20 J. I. Choi, H. Chun and M. S. Lah, *J. Am. Chem. Soc.*, 2018, **140**, 10915–10920.
21 M. B. Salamon, *Physics of Superionic Conductors*, Springer, Berlin, 1979.
22 D.-W. Lim and H. Kitagawa, *Chem. Rev.*, 2020, DOI: 10.1021/acs.chemrev.9b00842.
23 Y. Ye, L. Gong, S. Xiang, Z. Zhang and B. Chen, *Adv. Mater.*, 2020, (1–28), 1907090.
24 S. Wang, M. Wahiduzzaman, L. Davis, A. Tissot, W. Shepard, J. Marrot, C. Martineau-Corcos, D. Hamdane, G. Maurin, S. Devautour-Vinot and C. Serre, *Nat. Commun.*, 2018, **9**, 4937–4945.
25 M. Wahiduzzaman, S. Wang, J. Schnee, A. Vimont, V. Ortiz, P. G. Yot, R. Retoux, M. Daturi, J. S. Lee, J.-S. Chang, C. Serre, G. Maurin and S. Devautour-Vinot, *ACS Sustainable Chem. Eng.*, 2019, **7**, 5776–5783.
26 D. Frenkel and B. Smit, *Understanding Molecular Simulation: from Algorithms to Applications*, Academic Press, San Diego, 2002.
27 F. Salles, S. Bourrelly, H. Jobic, T. Devic, V. Guillerm, P. Llewellyn, C. Serre, G. Ferey and G. Maurin, *J. Phys. Chem. C*, 2011, **115**, 10764–10776.
28 D. D. Borges, S. Devautour-Vinot, H. Jobic, J. Ollivier, F. Nouar, R. Semino, T. Devic, C. Serre, F. Paesani and G. Maurin, *Angew. Chem., Int. Ed.*, 2016, **55**, 3919–3924.
29 P. G. M. Mileo, T. Kundu, R. Semino, V. Benoit, N. Steunou, P. L. Llewellyn, C. Serre, G. Maurin and S. Devautour-Vinot, *Chem. Mater.*, 2017, **29**, 7263–7271.
30 R. Mancinelli, A. Botti, F. Bruni, M. A. Ricci and A. K. Soper, *J. Phys. Chem. B*, 2007, **111**, 13570–13577.
31 D. C. Rapaport, *Mol. Phys.*, 1983, **50**, 1151–1162.
32 I. Skarmoutsos, M. Eddaoudi and G. Maurin, *J. Phys. Chem. C*, 2019, **123**, 26989–26999.
33 A. Weiss, N. Reimer, N. Stock, M. Tiemann and T. Wagner, *Phys. Chem. Chem. Phys.*, 2015, **17**, 21634–21642.
34 J. Zhang, L. Sun, C. Chen, M. Liu, W. Dong, W. Guo and S. Ruan, *J. Alloys Compd.*, 2017, **695**, 520–525.
35 Y. Gao, P. Jing, N. Yan, M. Hilbers, H. Zhang, G. Rothenberg and S. Tanase, *Chem. Commun.*, 2017, **53**, 4465–4468.
36 P. G. M. Mileo, K. Adil, L. Davis, A. Cadiau, Y. Belmabkhout, H. Aggarwal, G. Maurin, M. Eddaoudi and S. Devautour-Vinot, *J. Am. Chem. Soc.*, 2018, **140**, 13156–13160.
37 J. Zou, H. He, J. Dong and Y. Long, *J. Mater. Chem.*, 2004, **14**, 2405–2411.